Angle-dependent Andreev reflection at an interface with a polaritonic superfluid

I. Septembre,[1,*] D. D. Solnyshkov,[1,2] and G. Malpuech[1]
[1]*Université Clermont Auvergne, Clermont Auvergne INP, CNRS, Institut Pascal, F-63000 Clermont-Ferrand, France*
[2]*Institut Universitaire de France (IUF), 75231 Paris, France*

(Received 6 December 2022; revised 7 September 2023; accepted 8 September 2023; published 21 September 2023)

We study analytically an analog of the Andreev reflection at a normal-superfluid interface. The polariton gapped superfluid region is achieved by quasiresonant optical pumping. The interacting polaritons are described with the driven-dissipative Gross-Pitaevskii equation. We find analytical formulas for the angles and amplitudes of the reflected and transmitted particles. There are limit angles and energies, above which Andreev reflection and transmission cannot be observed anymore and where the Andreev wave becomes a surface mode, exponentially localized on the interface. These properties are confirmed by solving numerically the Gross-Pitaevskii equation in simulations reproducing realistic experimental conditions.

DOI: 10.1103/PhysRevB.108.115309

I. INTRODUCTION

Andreev reflection is an anomalous reflection occurring at the interface between a superconducting and a nonsuperconducting material [1]. An electron, instead of being reflected with just its direction changed, is reflected as a hole excitation. Its energy is inverted with respect to the Fermi energy, and so are its charge, wave vector, and spin. Inversely, an incoming hole is reflected as an electron. Andreev reflection determines the properties of metal/superconductor structures [2,3]. It has been observed experimentally not only in electronic systems [4,5] but also in superfluid helium experiments [6]. However, it has never been observed in fermionic gases despite a proposal [7,8] (we find that Ref. [9], despite interpreting transport properties as signatures of multiple Andreev reflection, is not a clear and direct measurement of the Andreev reflection in fermionic gases). The Andreev process can also lead to specular reflection when dealing with relativistic electron dispersion relations as in graphene [10].

A similar effect has been discovered and studied in the 1970s in nonlinear optics. It is known as optical phase conjugation [11], also related to optical parametric scattering. In this context, an incident optical wave arriving on a phase-conjugating mirror (which involves nonlinear processes) is reflected as its time-reversed partner, meaning that the reflected wave has the same frequency and opposite wave vector. The analogy between optical phase conjugation achieved using degenerate four-wave mixing and the electronic Andreev reflection has been noticed and discussed in Refs. [12,13]. Andreev reflection on a Bose-Einstein condensate has been proposed theoretically as well [14] but has not been observed yet. In Ref. [14], the Bose-Einstein condensate was in a supersonic regime. This allows one to draw a parallel with phenomena occurring close to the horizon of a black hole. It is now understood that Andreev reflection is very similar to phenomena encountered near the horizon of black holes [15–19], such as Hawking emission. The study of Hawking emission analog [20] using quantum fluids either made of atomic vapors or of light became a very active research field in the last years both theoretically and experimentally [21–28].

Exciton-polaritons are quasiparticles arising from the strong coupling of excitons and cavity photons [29]. They exhibit strong interactions, and thus a polariton mode behaves as a nonlinear oscillator exhibiting bistability [30]. Exciton-polaritons are part-light part-matter bosonic quasiparticles arising from the strong coupling between semiconductor excitons and confined photons [31,32]. They are intrinsically strongly interacting and their bosonic nonlinearity can show up as a parametric oscillator behavior [33–40] or Bose-Einstein condensation [41–45] even at room temperature [46–50]. Polaritons also offer broad possibilites for analog gravity simulations [23]. Under resonant pumping, the spectrum of the elementary excitations of the pumped mode is complex because of the driven dissipative nature of the system. However, above the bistability threshold it contains a gap between the real parts of eigenenergies [32,51–55] showing similarities with the one of a superconductor. In this regime the excitation of the fluid approximately verifies the Landau criterion of superfluidity, the remaining dissipation being due to the imaginary part of bogolon energies [56,57]. This regime can therefore be called a gapped superfluid regime where the pumped mode shows original rigid behavior against perturbations [54]. In a previous work, we have considered the reflection of a plane wave at an energy $E + E_p$ on such superfluid of energy E_p and phase ϕ [39]. We have shown that normal elastic reflection occurs together with an Andreev reflection analog at an energy $E_p - E$ and with a phase shift 2ϕ. This Andreev reflection phenomenon can be interpreted using nonlinear optics vocabulary as the result of a parametric scattering process. We have shown that the phase shift 2ϕ can be interpreted as an artificial gauge field allowing the implementation of topological bands in multi-terminal Josephson junctions [58].

In this work, we go further and study comprehensively the angular dependence of the Andreev reflection on a polaritonic gapped superfluid in two dimensions (2D). We

*Corresponding author: ismael.septembre@uca.fr

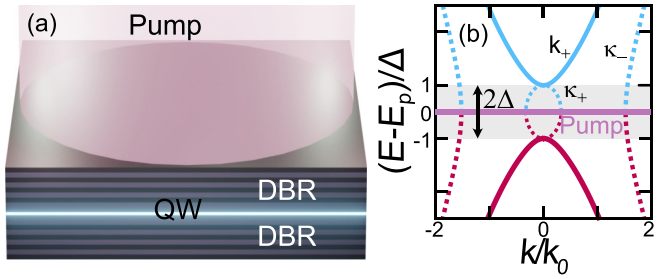

FIG. 1. (a) Sketch of the planar optical microcavity hosting exciton-polaritons. Light is confined in the z direction by distributed Bragg reflectors (DBR), while excitons are confined by a quantum well (QW). The external pumping is provided by a laser at energy E_p. (b) Energy dispersion of the propagative states (solid lines) associated with the wave vector k_+ and energy dependence of the inverse decay lengths (dotted lines) $\kappa_\pm$ in the gapped superfluid regime. The gap is the shaded area where no propagative states exist, and is centered around the pump energy (purple line). Blue—positive energy $+E$; red—negative energy $-E$. $k_0 = \sqrt{2mE_\mathrm{p}}/\hbar$.

derive the Bogoliubov-de Gennes equations from the 2D Gross-Pitaevskii equation for a 2D planar microcavity hosting exciton-polaritons with quasiresonant pumping. The interface between a nonsuperfluid region (not pumped) and a gapped superfluid region (pumped) is the theatre of an anomalous reflection, similar to the Andreev reflection, and a nontrivial transmission (for energies of incident particles larger than the gap). We solve the problem analytically, finding the different quantities characterizing the reflection and the transmission, such as wave vectors and decay lengths, angles, critical angles and energies, and the scattering coefficients. We moreover find peculiar solutions that take the form of surface modes for the Andreev wave. The analytical results are verified by solving numerically the 2D Gross-Pitaevskii equations. These results can be useful to study polaritonic multiterminal Josephson junctions that host Weyl singularities [58] and also in the study of phenomena occurring close to the horizon of black holes.

II. GAPPED SUPERFLUID REGIME

In this section, we consider a planar microcavity hosting interacting photons (exciton-polaritons) under quasiresonant pumping. We neglect polarization effects. We remind the existence of a gapped superfluid regime and the subsequent elementary excitations of the system (bogolons). An originality here is that we consider both the well-known propagative states and the spatially decaying evanescent solutions which, in particular, exist in the gap and which are important to describe the reflection processes at the gap energies. We study a strongly coupled planar microcavity [32,53,59] composed of two distributed Bragg reflectors surrounding a quantum well, as depicted in Fig. 1(a).

This type of cavity allows confining exciton-polaritons in the z direction, letting them propagate in the (x, y) plane where they can be described by a parabolic dispersion relation. We first consider the situation where the whole cavity is under quasiresonant pumping. Experimentally, a pump laser drives the whole cavity from the top, as shown in Fig. 1(a). The wave function ψ of a quasiparticle confined in the cavity can be described using the 2D Gross-Pitaevskii equation:

$$i\hbar\frac{\partial\psi}{\partial t} = \left[-\frac{\hbar^2}{2m}\nabla^2 - i\gamma + \alpha|\psi|^2\right]\psi + P, \tag{1}$$

where $\hbar$ is the reduced Planck constant, m the effective mass of the exciton-polaritons, γ their lifetime, $\alpha > 0$ the repulsive interaction between them, and $P = P_0 e^{-i\omega_p t}$ the pumping term at the energy $E_\mathrm{p} = \hbar\omega_p$ (we consider the laser pump to be at normal incidence). P_0 is the amplitude of the pump. We consider $\gamma \to 0$ to simplify the analytics, but we verify the validity of the solutions obtained with this assumption later. A nonzero decay shows up in the imaginary part of the bogolon energy, but does not qualitatively affect our results in this configuration. This equation has a spatially homogeneous solution $\psi_s = \sqrt{n}e^{i\phi}$ demonstrating a bistable behavior [30]. The density of exciton-polaritons $|\psi|^2 = n$ can be directly measured experimentally because it dictates the intensity of the light emitted by the cavity. Additionally to the spatially homogeneous solution, we consider the weak superfluid excitations called bogolons which result from the nonlinear coupling between two complex conjugate particles:

$$\psi = e^{-i\omega_p t}(\psi_s + ue^{i\mathbf{kr}}e^{-i\omega t} + v^* e^{-i\mathbf{kr}}e^{i\omega^* t}), \tag{2}$$

where u, v are the Bogoliubov coefficients. We can obtain the Bogoliubov-de Gennes equations by inserting the wave function (2) into the Gross-Pitaevskii equation (1):

$$\begin{pmatrix} \mathcal{L} & \alpha\psi_s^2 \\ -\alpha\psi_s^{*2} & -\mathcal{L}^* \end{pmatrix}\begin{pmatrix} u \\ v \end{pmatrix} = E\begin{pmatrix} u \\ v \end{pmatrix}, \tag{3}$$

where $\mathcal{L} = (\epsilon_\mathbf{k} - E_\mathrm{p} + 2\alpha n)$ with $\epsilon_k = \hbar^2k^2/2m$ ($|\mathbf{k}| = k$). $E = \hbar\omega$ denotes the energy of a particle with respect to the pump energy E_p. The energy E comes straightforwardly from Eq. (3):

$$E^2 = (\epsilon_\mathbf{k} + \alpha n - E_\mathrm{p})(\epsilon_\mathbf{k} + 3\alpha n - E_\mathrm{p}). \tag{4}$$

One can use Eq. (4) to determine the wave vectors of the particles depending on their energy:

$$k_\pm = \frac{\sqrt{2m(E_\mathrm{p} - 2\alpha n \pm \sqrt{(\alpha n)^2 + E^2})}}{\hbar}. \tag{5}$$

If we only consider the case of repulsive interactions $\alpha n > 0$, then there are four different configurations of the system. First, the superfluid regime is obtained when $\alpha n \geqslant E_\mathrm{p}$. The limit case $\alpha n = E_\mathrm{p}$ gives the linear Bogoliubov spectrum, equivalent to the one found in the case of thermal equilibrium $\mu = \alpha n$, which is $E^2 = \epsilon_k(\epsilon_k + 2\alpha n)$. Then, for $\alpha n > E_\mathrm{p}$, the superfluid is gapped, meaning that the two branches of the dispersion are separated by a gap 2Δ, centered at the pump energy, with

$$\Delta = \sqrt{(\alpha n - E_\mathrm{p})(3\alpha n - E_\mathrm{p})}. \tag{6}$$

In addition to these two superfluid regimes, where one can find the dispersion relation of excitations with completely real energies, there are different cases for $E_\mathrm{p} > \alpha n > 0$ where the dispersion relation is complex, including rings of exceptional points (non-Hermitian degeneracy line [60–66]). We will not consider these configurations in the following. We study only

the gapped superfluid configuration where $\alpha n > E_p$. We consider not only propagative states but also evanescent solutions (with imaginary wave vectors). Indeed, from Eq. 5, we see that the condition $\alpha n > E_p$ gives imaginary wave vectors (that is, evanescent states) for a range of energies. More precisely, the wave vector k_- is imaginary for all energies and the wave vector k_+ is real only for $|E| > \Delta$. This means that instead of the wave vectors (5), one should use inverse decay lengths:

$$\kappa_\pm = \sqrt{\frac{2m(2\alpha n - E_p \mp \sqrt{(\alpha n)^2 + E^2})}{\hbar^2}}, \tag{7}$$

which are the direct extensions of $k_\pm$, respectively, to the case of imaginary wave vectors.

We plot the dispersion relation of the propagative states and the dependence of the inverse decay lengths on the energy in Fig. 1(b). The dispersion relation obtained from Eq. (4) shows propagative states (solid lines) that correspond to real energies and demonstrate a gap. There are also evanescent states, associated with κ_+ (for $|E| < \Delta$) and κ_- (for all energies). The dispersion relation of these states is shown in dashed lines in Fig. 1(b). When the energy of a particle lies inside the gap $|E| < \Delta$, there are only evanescent states in the superfluid. However, we insist that the evanescent states are present in the superfluid even outside the gap, together with the propagative states: they are important to describe the interfaces in finite-size systems, as we will see below.

The parts of the wave function oscillating at frequencies $\pm E/\hbar$ are determined by the Bogoliubov coefficients u, v. They can be found from Eq. (3) with an appropriate normalization condition. A bogolon is a particle of energy E' (which can be positive or negative) with fractions $|u|^2$ at E and $|v|^2$ at $-E$. We choose $E > 0$, and consider two normalization conditions: $|u|^2 - |v|^2 = 1$ and $|u|^2 - |v|^2 = -1$. Considering $E < 0$ would just lead to the same set of solutions with inverted meaning of u and v. Therefore,

$$E' = E|u|^2 - E|v|^2$$

with

$$\begin{aligned} |u|^2 - |v|^2 = 1 \;&\Rightarrow\; E' = E > 0, \\ |u|^2 - |v|^2 = -1 \;&\Rightarrow\; E' = -E < 0. \end{aligned} \tag{8}$$

The analytical formulas of the coefficients can be computed from Eqs. (3) and (8):

$$\begin{aligned} u_\pm &= \frac{\sqrt{\sqrt{(\alpha n)^2 + E^2} \pm E}}{\sqrt{2E}} e^{i\phi}, \\ v_\pm &= \pm \frac{\sqrt{\sqrt{(\alpha n)^2 + E^2} \mp E}}{\sqrt{2E}} e^{-i\phi}, \end{aligned} \tag{9}$$

Note that the phase of the superfluid ϕ appears in the Bogoliubov coefficients with opposite signs (positive in u and negative in v), which can be traced back to the conjugation in Eq. (2).

Now that we have provided a detailed study of the different regimes achievable for a collective excitation of the gapped superfluid formed by quasiresonant pumping of an optical microcavity, we can proceed to the description of systems containing interfaces.

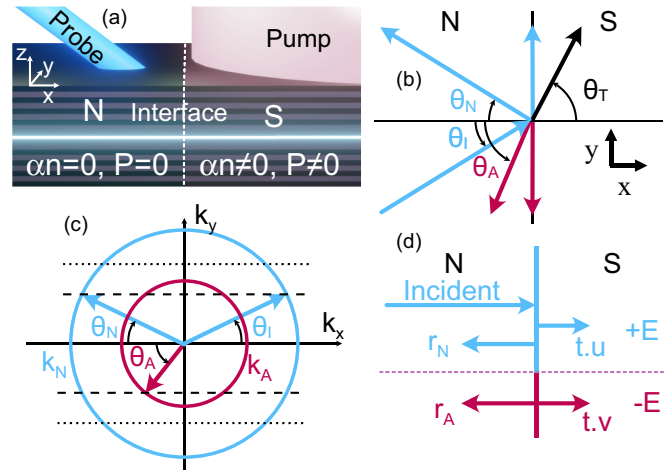

FIG. 2. (a) Scheme of the cavity hosting exciton-polaritons, partly under resonant pumping creating a superfluid (red) region. A probe (blue) is sent from the normal region toward the interface (white dotted line) to observe Andreev reflection. (b) Scheme of the 2D real space for an incident wave at positive energy. The arrows denote the wave vectors with angle $\theta_{I,N,A,T}$ (with respect to the normal incidence) denoting incident, normally reflected, Andreev reflected, and transmitted wave at positive (blue) and negative (red) energies. (c) Scheme of the k-space where the norms $k_{N,A}$ appear as circles, the radius of the latter being smaller. This allows finding the angles because of the constant k_y (dashed/dotted black lines). For a given k_y (set by E and θ_I), Andreev reflection can be possible (dashed) or impossible (dotted black lines). (d) Energy representation of the scattering phenomena. A wave incident at positive energy is reflected both at the same energy and at its opposite (and is transmitted at both energies if $|E| > \Delta$).

III. ANDREEV REFLECTION ANALOGUE

We now consider a different configuration where only half of the cavity is pumped, as shown in Fig. 2(a). This creates an interface between the area under pumping and the area without pumping, that is, a normal-superfluid interface. We show that a phenomenon analogous to Andreev reflection can occur at this interface, and study its properties.

In our model, the interaction and pumping terms present a step-like profile, as shown in Fig. 2(a). The interactions and pumping are null for $x < 0$ and constant for $x > 0$, which sets a sharp interface at $x = 0$ between the two regions. The $x > 0$ region is in the gapped superfluid regime $\alpha n > E_p$. For the normal region $x < 0$, where there are no interactions nor pumping, Eq. (1) reduces to the 2D time-dependent Schrödinger equation:

$$i\hbar \frac{\partial \psi}{\partial t} = -\frac{\hbar^2}{2m} \Delta \psi \tag{10}$$

with plane waves solutions of the form:

$$\psi(x < 0, y, t) = e^{i\mathbf{k}.\mathbf{r}} e^{-i\epsilon_k t/\hbar} \tag{11}$$

with:

$$\epsilon_k = \frac{\hbar^2 k^2}{2m}. \tag{12}$$

On the contrary, for $x > 0$, the complete form of Eq. (1) has to be used. We will consider the problem of a wave incident from the normal region on the superfluid region. However, depending on whether the particle has its energy inside or outside the gap, the wave function ansatz will be different, describing evanescent or propagative states in the superfluid. We first consider the case of energies of incident particles lying inside the gap $|E| < \Delta$, so that there can be no propagation in the superfluid, and therefore there is no transmission. This is a nontrivial extension of the previous 1D study in [39] to two dimensions. Then we consider energies outside the gap, leading to propagative states in the superfluid region.

A. $|E| < \Delta$

We consider the problem of an incident particle of energy $0 < E < \Delta$ (the derivation made for an incident particle of energy $-E$ follows the same lines). Because we measure energies with respect to the pump energy, the norm of the wave vector is:

$$k_N = \frac{\sqrt{2m(E_\mathrm{p} + E)}}{\hbar}. \tag{13}$$

If the incident wave has an angle of incidence θ_I ($0 \leqslant \theta_I < \pi/2$) from the normal region toward the superfluid one, then its wave vector is

$$\mathbf{k}_I = k_N(\cos\theta_I \mathbf{x} + \sin\theta_I \mathbf{y}). \tag{14}$$

The wave vector along y denoted k_y is thus determined completely by the angle of incidence and the energy of the incident particles, that is, by two parameters that can be easily tuned in experiments with polaritons. Its expression is

$$k_y = k_N \sin\theta_I. \tag{15}$$

The invariance of the problem in the y direction imposes that at a given energy the wave vector along y is the same in the normal region and the superfluid. All waves at the energy E of the incident wave possess the same y component of the wave vector k_y. At the energy of the Andreev reflection, symmetric to E with respect to E_p, the y component of the wave vector is $-k_y$ because of the complex conjugation resulting from the parametric processes creating amplitudes at the Andreev energy. To use the scattering formalism, we need to define the different scattering states we will consider. First, we consider the incident wave

$$\psi_I = \begin{pmatrix} 1 \\ 0 \end{pmatrix} e^{ik_N x \cos\theta_I} e^{ik_y y}, \tag{16}$$

using the following basis to describe the two conjugate frequencies:

$$e^{-iE/\hbar t} \equiv \begin{pmatrix} 1 \\ 0 \end{pmatrix}; \; e^{+iE/\hbar t} \equiv \begin{pmatrix} 0 \\ 1 \end{pmatrix}. \tag{17}$$

This unique incident wave provokes two different reflections. The first one is the normal reflection whose wave function reads

$$\psi_N = \begin{pmatrix} 1 \\ 0 \end{pmatrix} e^{ik_N \cos\theta_N x} e^{ik_y y}, \tag{18}$$

and the second one is the Andreev-like reflection with a wave vector:

$$k_A = \frac{\sqrt{2m(E_\mathrm{p} - E)}}{\hbar}. \tag{19}$$

This corresponds to a wave with reversed energy (with respect to the pump energy). Its wave function reads

$$\psi_A = \begin{pmatrix} 0 \\ 1 \end{pmatrix} e^{ik_A \cos\theta_A x} e^{-ik_y y}. \tag{20}$$

The relations between the different angles can be determined from the translational invariance of the problem along the y direction, which yields [1]

$$k_y = k_N \sin\theta_I = -k_N \sin\theta_N = k_A \sin\theta_A. \tag{21}$$

This gives both the trivial result $\theta_N = -\theta_I$ and the nontrivial result

$$\theta_A = \arcsin\left(\frac{k_N}{k_A}\sin\theta_I\right). \tag{22}$$

This is analogous to the Snell-Descartes law, which has already been extended to interfaces of electronic systems [67,68]. However, there is no minus sign for the angle of the Andreev reflection, meaning that it occurs in the direction opposite to the incident wave. The different angles considered $\theta_{I,N,A}$ are represented in real space in Fig. 2(b) and in reciprocal space in Fig. 2(c). The Andreev reflection occurs in the same quadrant as the incident wave, which is very different from the usual reflection, but close to the electronic Andreev reflection. In our case, however, the so-called Andreev approximation does not hold. In electronics, this approximation states that the Andreev-reflected particle has a direction strictly reversed with respect to the incident particle because the gap Δ is negligible with respect to the Fermi energy $\Delta \ll E_\mathrm{F}$. In our case, the pump detuning E_p plays the role of the Fermi energy $E_\mathrm{F} \sim E_\mathrm{p}$. The Andreev approximation in our case would consist in neglecting Δ with respect to E_p. However, in our system, the gap can be approximately equal to the pump detuning $\Delta \approx E_\mathrm{p}$ ($2\Delta = E_\mathrm{p}$ in most of the figures). Moreover, the expression of the angle clearly states that for incident particles of positive energies (still with respect to E_p), the Andreev-reflected particle will be reflected at a higher angle, giving upper bound for the angle of incidence $\theta_{I,Rc}$, above which no Andreev reflection is possible:

$$\theta_{I,Rc} = \arcsin\sqrt{\frac{E_\mathrm{p} - E}{E_\mathrm{p} + E}}. \tag{23}$$

Above this angle, the Andreev wave becomes a surface wave, evanescent on both sides of the interface.

On the contrary, if the energy of the incident particle is negative, then the Andreev-reflected particle will be reflected at an angle smaller than the angle of incidence: $\theta_A \leqslant \theta_I$. There will be no limit angle in that case because for normal incidence $\theta_I = 0$ the Andreev reflection will be normal as well. The dependence of the deviation of the angle of Andreev

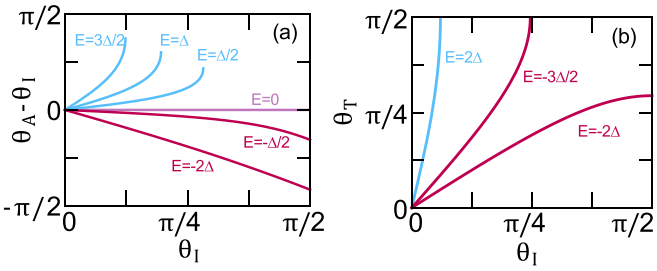

FIG. 3. (a) Andreev reflection angle with respect to the angle of incidence for different energies of the incident wave. The difference is not negligible, because the Andreev approximation ($\Delta \ll E_p$) does not hold. (b) The angle of the transmitted wave with respect to the angle of incidence for different energies of the incident wave.

reflection from the angle of incidence $\theta_A - \theta_I$ on the angle of incidence θ_I for different energies is plotted in Fig. 3(a). We can see that for positive energies, the curves exhibit a limit angle, whereas for negative energies there is no such bound, as stated above.

Now that the different propagative states are defined in the normal region, we can consider the scattering process of Andreev reflection and compute the scattering coefficients. In the case $|E| < \Delta$, there are no propagative states in the superfluid, so the wave function of the collective excitation in the superfluid (2) has to be written explicitly to account for the exponential spatial decay of the evanescent states:

$$\psi(x > 0, y, t) = e^{-i\omega_p t}(\psi_s + ue^{ik_y y}e^{-\kappa x}e^{-i\omega t} + v^* e^{-ik_y y}e^{-\kappa x}e^{i\omega t}). \quad (24)$$

We consider only real frequencies. κ is the inverse decay length and k_y is the wave vector in the y direction, directly inherited from the incident wave. The propagative form of this term is responsible for the shift of finite-size beams upon reflection in the Goos-Hänchen effect [69] and its analogs.

Inserting the solution (24) into the equation (1) we find

$$E^2 = (\epsilon_{k_y} - \epsilon_{\kappa_x} + \alpha n - E_p)(\epsilon_{k_y} - \epsilon_{\kappa_x} + 3\alpha n - E_p). \quad (25)$$

From this relation, we can find that there are two different inverse decay lengths at each energy, different from the spatially homogeneous case of Eq. (7) because it takes into account the interface and the invariance along y:

$$\kappa_\mp = \sqrt{k_y^2 + \frac{2m(2\alpha n - E_p \pm \sqrt{(\alpha n)^2 + E^2})}{\hbar^2}}. \quad (26)$$

We define the scattering matrix in the $\{E, -E\}$ basis as

$$S = \begin{pmatrix} r_N & r_A^* \\ r_A & r_N \end{pmatrix}, \quad (27)$$

where $r_{N,A}$ are the scattering coefficients denoting normal/Andreev reflection, respectively. To determine them, we consider the wave functions in the normal region Ψ_N and superfluid region Ψ_S for a given configuration, say an incident wave from the normal region toward the interface at positive energy. This gives

$$\Psi_N = \frac{1}{\sqrt{w_+}}(\psi_I + r_N\psi_N) + \frac{1}{\sqrt{w_-}}r_A\psi_A, \quad (28)$$

where $w_\pm = \frac{\hbar}{m}k_{N,A}\cos\theta_{I,A}$ are the group velocities in the x direction at $\pm E$, and

$$\Psi_S = \sum_{*\equiv\pm} \eta_* e^{-\kappa_* x}\begin{pmatrix} u_* e^{ik_y y} \\ v_* e^{-ik_y y}\end{pmatrix}. \quad (29)$$

The use of the group velocities is mandatory to conserve the density current in the x direction.

The scattering coefficients are found from the continuity of the wave function and its derivative at the interface for both energies, which gives a system of equations:

$$\Psi_N(x=0) = \Psi_S(x=0)$$
$$\frac{\partial\Psi_N}{\partial x}(x=0) = \frac{\partial\Psi_S}{\partial x}(x=0), \quad (30)$$

which can be written in a complete form composed of four equations:

$$\frac{1}{\sqrt{w_+}}[1+r_N]e^{ik_y y}\begin{pmatrix}1\\0\end{pmatrix} + \frac{r_A}{\sqrt{w_-}}e^{-ik_y y}\begin{pmatrix}0\\1\end{pmatrix} = \eta_+\begin{pmatrix}u_+e^{ik_y y}\\ v_+e^{-ik_y y}\end{pmatrix} + \eta_-\begin{pmatrix}u_-e^{ik_y y}\\ v_-e^{-ik_y y}\end{pmatrix}, \quad (31)$$

$$\frac{ik_N\cos\theta_I}{\sqrt{w_+}}[1-r_N]e^{ik_y y}\begin{pmatrix}1\\0\end{pmatrix} - \frac{ik_A\cos\theta_A r_A}{\sqrt{w_-}}e^{-ik_y y}\begin{pmatrix}0\\1\end{pmatrix} = -\kappa_+\eta_+\begin{pmatrix}u_+e^{ik_y y}\\ v_+e^{-ik_y y}\end{pmatrix} - \kappa_-\eta_-\begin{pmatrix}u_-e^{ik_y y}\\ v_-e^{-ik_y y}\end{pmatrix}. \quad (32)$$

The normal and Andreev reflection coefficients are then determined analytically:

$$r_N = \frac{(k_A\cos\theta_A + i\kappa_-)(k_N\cos\theta_I - i\kappa_+)u_+v_- - (k_N\cos\theta_I - i\kappa_-)(k_A\cos\theta_A + i\kappa_+)u_-v_+}{(k_A\cos\theta_A + i\kappa_-)(k_N\cos\theta_I + i\kappa_+)u_+v_- - (k_N\cos\theta_I + i\kappa_-)(k_A\cos\theta_A + i\kappa_+)u_-v_+}, \quad (33)$$

$$r_A = \frac{2ik_N\cos\theta_I(\kappa_+ - \kappa_-)v_-v_+}{(k_A\cos\theta_A + i\kappa_-)(k_N\cos\theta_I + i\kappa_+)u_+v_- - (k_N\cos\theta_I + i\kappa_-)(k_A\cos\theta_A + i\kappa_+)u_-v_+}\frac{\sqrt{w_-}}{\sqrt{w_+}}. \quad (34)$$

In the end, all the quantities can be calculated from the experimental conditions. As shown in Fig. 2(d), a unique incident wave gives indeed two different reflections (for $\theta_I < \theta_{I,Rc}$). The first one (specular reflection) is at the energy of the incident wave, with an amplitude r_N. The second one (Andreev reflection) is at the conjugate frequency, with an amplitude r_A. There is no transmission in the superfluid, only evanescent states. The profile of the corresponding wave

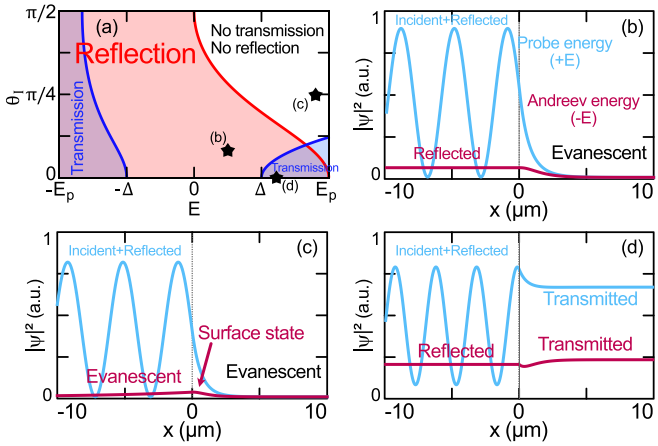

FIG. 4. (a) Phase diagram showing the experimental conditions E, θ_I leading to Andreev reflection (red) and/or transmission (blue areas). The domains are limited by red/blue thick lines, respectively. (b–d) Real space profile of the states at positive (blue) and negative (red) energy for three different experimental conditions. (b) $\theta_I = \pi/6$, $E = \Delta/2 = 0.125\,\text{meV}$ leads to Andreev reflection but no transmission, all states are evanescent in the superfluid. (c) $\theta_I = \pi/4$, $E = 0.45\,\text{meV}$, where there are only evanescent states at the negative energy, which creates a surface state. (d) $\theta_I = 0$, $E = 0.3\,\text{meV}$, which give both an Andreev reflection and transmission in the superfluid. Note that specular reflection is present in all cases, which leads to interferences (with the incident probe) in the amplitude at positive energy in the normal region.

function in real space is plotted in Fig. 4(b). The incident and reflected waves at the incident frequency (blue) interfere, leading to a spatial modulation of the wave function at positive energy on the left-hand side of the interface ($x < 0$, normal region). On the contrary, there is only one reflected wave at the Andreev frequency (in red), which gives a constant profile in the normal region. In the superfluid region, at both energies, the states are evanescent and the norm of the wave functions rapidly decreases to zero. Above the limit angle, the Andreev reflection coefficient goes to zero, meaning that Andreev reflection cannot occur anymore, because the wave vector k_y dictated by experimental conditions is larger than k_A [see Fig 2(c), in the case of the black dotted line]. If Andreev reflection is impossible, then the profiles of the wave functions will look as shown in Fig. 4(c). At positive energy, this is very similar to the case of Fig. 4(b), but at negative energy, Andreev reflected waves cannot propagate in the normal region and are evanescent, as well as in the superfluid. In the end, the state at negative energy is evanescent at both sides of the interface, so it is a surface state exponentially localized at the interface.

B. $|E| > \Delta$

Previously, we considered only the case $|E| < \Delta$, that is, energies lying inside the gap. However, Andreev reflection can occur even outside the gap. The derivation is very similar to what was shown previously. However, one should work with the propagative states in the superfluid, with the wave vectors (5) (we remind that even for $|E| > \Delta$, there are still evanescent states in the superfluid in addition to the propagative states, describing the wave profile close to the interface). The particle is transmitted at an angle of

$$\theta_\text{T} = \arcsin\left(\frac{k_\text{N}}{k_\text{T}}\sin\theta_\text{I}\right), \tag{35}$$

determined by $k_y = k_N \sin\theta_I = k_T \sin\theta_T$, where $k_T \equiv k_+$ is the wave vector of the transmitted particle. Since $k_T > k_N$, there is a critical angle of incidence above which there is no transmission, even for $|E| > \Delta$:

$$\theta_{I,Tc} = \arcsin\left(\frac{E_\text{p} - 2\alpha n + \sqrt{(\alpha n)^2 + E^2}}{E_\text{p} + E}\right). \tag{36}$$

Figure 3(b) shows the angle of transmission with respect to the angle of incidence for different energies. Again, there is a critical angle for certain energies, when θ_T reaches the value $\pi/2$, as shown in this figure.

We represented the domains of energy/angle of incident particle where Andreev reflection (red) or transmission (blue) is possible in Fig. 4(a) using Eqs (23) and (36). We see that the effective gap $\tilde{\Delta}$ where no transmission is possible is equal to the gap Δ calculated in Eq. (6) only for $\theta_I = 0$. Away from normal incidence, the effective gap is much larger than this value, meaning that the transmission is possible only for small angles of incidence.

Moreover, in the region $|E| > \Delta$ the scattering coefficients change with respect to those computed for $|E| < \Delta$, and there is one more scattering coefficient to determine, the one accounting for the transmission in the superfluid. We can write the wave function in the superfluid in this case:

$$\Psi_{S,t} = t\begin{pmatrix} u_+ e^{i(k_+ x + k_y y)} \\ v_+ e^{-i(k_+ x + k_y y)} \end{pmatrix} + \eta_- e^{-\kappa_- x}\begin{pmatrix} u_- e^{ik_y y} \\ v_- e^{-ik_y y} \end{pmatrix}, \tag{37}$$

and we finally find the transmission coefficient by considering the continuity of the wave function and its derivative at the interface:

$$r_N = \frac{(k_A\cos\theta_A + i\kappa_-)(k_N\cos\theta_I - k_T\cos\theta_T)u_+v_- - (k_N\cos\theta_I - i\kappa_-)(k_A\cos\theta_A - k_T\cos\theta_T)u_-v_+}{(k_A\cos\theta_A + i\kappa_-)(k_N\cos\theta_I + k_T\cos\theta_T)u_+v_- - (k_N\cos\theta_I + i\kappa_-)(k_A\cos\theta_A - k_T\cos\theta_T)u_-v_+}, \tag{38}$$

$$r_A = \frac{2k_N\cos\theta_I(k_T\cos\theta_T + i\kappa_-)v_-v_+}{(k_A\cos\theta_A + i\kappa_-)(k_N\cos\theta_I + k_T\cos\theta_T)u_+v_- - (k_N\cos\theta_I + i\kappa_-)(k_A\cos\theta_A - k_T\cos\theta_T)u_-v_+}\frac{\sqrt{w_-}}{\sqrt{w_+}}, \tag{39}$$

$$t = \frac{2k_N\cos\theta_I(k_A\cos\theta_A + i\kappa_-)v_-}{(k_A\cos\theta_A + i\kappa_-)(k_N\cos\theta_I + k_T\cos\theta_T)u_+v_- - (k_N\cos\theta_I + i\kappa_-)(k_A\cos\theta_A - k_T\cos\theta_T)u_-v_+}\frac{\sqrt{w_T}}{\sqrt{w_+}}, \tag{40}$$

where $w_T = \xi \hbar k_T \cos\theta_T/m$ is the group velocity for waves transmitted in the superfluid, with $\xi = (2\alpha n - E_\mathrm{p} + \epsilon_k)/E$. Using $u_+ = -v_- e^{2i\phi}$ and $v_+ = u_- e^{2i\phi}$, we can rewrite these expressions as

$$r_N = \frac{(k_A\cos\theta_A + i\kappa_-)(k_N\cos\theta_I - k_T\cos\theta_T)v^2 + (k_N\cos\theta_I - i\kappa_-)(k_A\cos\theta_A - k_T\cos\theta_T)u^2}{(k_A\cos\theta_A + i\kappa_-)(k_N\cos\theta_I + k_T\cos\theta_T)v^2 + (k_N\cos\theta_I + i\kappa_-)(k_A\cos\theta_A - k_T\cos\theta_T)u^2}, \tag{41}$$

$$r_A = \frac{2\sqrt{k_N k_A}\cos\theta_I(k_T\cos\theta_T + i\kappa_-)uv}{(k_A\cos\theta_A + i\kappa_-)(k_N\cos\theta_I + k_T\cos\theta_T)v^2 + (k_N\cos\theta_I + i\kappa_-)(k_A\cos\theta_A - k_T\cos\theta_T)u^2}e^{-2i\phi}, \tag{42}$$

$$t = \frac{2\sqrt{k_N k_T}\cos\theta_I(k_A\cos\theta_A + i\kappa_-)v}{(k_A\cos\theta_A + i\kappa_-)(k_N\cos\theta_I + k_T\cos\theta_T)v^2 + (k_N\cos\theta_I + i\kappa_-)(k_A\cos\theta_A - k_T\cos\theta_T)u^2}e^{-i\phi}, \tag{43}$$

with $u = |u_-|$ and $v = |v_-|$. We will explain a few features of these scattering coefficients. First, one can verify that

$$|r_N|^2 + |r_A|^2\mathcal{U}(\theta_{I,Rc} - \theta_I) + |t|^2\mathcal{U}(|E| - \tilde{\Delta}) = 1, \tag{44}$$

where $\mathcal{U}$ denotes the Heaviside step function. This equation accounts for the conservation of the current density: an incident wave of amplitude 1 is partly reflected at the same frequency with amplitude $|r_N|^2$, partly at the conjugate frequency with amplitude $|r_A|^2$ (if the angle of incidence $\theta_I < \theta_{I,Rc}$), and partly transmitted with amplitude $|t|^2$ (if the energy $|E| > \tilde{\Delta}$) by a wave combining both frequencies. Moreover, we can see that the phase of the superfluid plays a role only in the components at $-E$. Indeed, it does not appear in r_N, but only in r_A (with a factor 2) and in t. The wave function transmitted in the superfluid is proportional to tu at E and tv at $-E$ [see Fig. 2(d)], which means that the total phase of the transmitted wave is 0 at E and -2ϕ at $-E$, in agreement with the phase matching condition of the parametric process discussed below and shown in Fig. 5(b).

We already discussed that there are experimental conditions leading to the presence of Andreev reflection and the absence of transmission [Fig. 4(b)], or to the absence of both Andreev reflection and transmission, accompanied by the formation of a surface wave [Fig. 4(c)]. As shown above, there are also experimental conditions where the transmission (and eventually Andreev reflection) can be observed. The profile of the state in this case is shown in Fig. 4(d): there is a transmission in the superfluid, and simultaneously evanescent states in the superfluid, as stated previously, whose influence on the profile is visible only close to the interface. Far from the interface, there is one plane wave at each energy, as expected from the form of the wave function (37). This is the propagative bogolon quasiparticle, with a part at positive and a part at negative energy, whose respective amplitudes are determined by u and v.

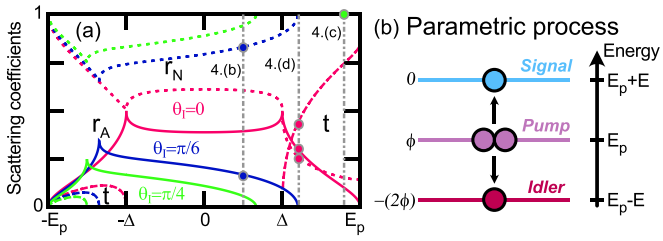

FIG. 5. (a) Scattering coefficients r_N (dotted), r_A (solid), and t (dashed lines) with respect to the energy for different angles of incidence $\theta_I = \{0, \pi/6, \pi/4\}$ in pink, blue, and green, respectively. The gray lines (and corresponding points) show the energy (and corresponding angles) for which are calculated the states in Fig. 4. Note the peaks in the remaining coefficients when one vanishes. (b) Illustration of the parametric process in Andreev reflection. The pump is at energy E_p with phase ϕ. Positive energies are at $E_\mathrm{p} + E$ with no phase (we disregard the phase of the incident wave) whereas negative energies at $E_\mathrm{p} - E$ gain a phase -2ϕ because of the parametric process [the minus sign appears because of the conjugation, see Eq. (2)]. Two "particles" from the pump are converted in one "particle" at $+E$ and no phase and one "particle" at $-E$ with a phase -2ϕ according to the phase-matching condition (45).

Figure 5(a) shows the variation of the scattering coefficients r_N, r_A, and t for an incident wave of energy $-E_\mathrm{p} < E < E_\mathrm{p}$ and with an angle of incidence θ_I (different angles are plotted with different colors). Increasing the angle of incidence generally decreases the Andreev reflection and transmission coefficients (the normal reflection thus increases, because the sum of all square norms of the scattering coefficients always equals 1). At $\theta_I = \pi/4$, r_A cancels for some frequency range within the gap. Here the mode at Andreev frequency is evanescent both in the superfluid and normal region, forming a propagating surface wave. It is clear that the particle-hole symmetry (mapping from E to $-E$) only holds for $|E| < \Delta$ and at normal incidence, so it is a very fragile case. Moreover, some coefficients exhibit infinite derivatives, which correspond to the appearance or disappearance of another coefficient. For instance, for $\theta_I = 0$ and $E = \Delta$, there is a peak with an infinite derivative for both the normal and Andreev reflections, r_N and r_A. For $E \to \Delta^-$, the inverse decay length $\kappa_+ \to 0$. Thus, the associated wave is less and less vanishing, which enhances the probability of energy conversion to occur, thus increasing the Andreev reflection (and decreasing the normal reflection at the same time). Reversely, for $E \to \Delta^+$, the wave vector $k_T \to 0$, and the wave propagates critically slowly in the superfluid (we remind that the dispersion relation of the gapped superfluid is parabolic), which again enhances the probability of energy conversion. Finally, for large energies $E \gg \Delta$, the transmission in the superfluid region becomes dominant over reflection.

In Fig. 5(a) we also indicate the regimes corresponding to the previous figures. First, we have considered the case of a wave incident at positive energy $E = 1.2\Delta$, and at normal incidence $\theta_I = 0$. This corresponds to the vertical gray line at this energy and the pink curves in Fig. 5(a). The gray line cuts the three pink curves when none of them is zero, meaning that there is a specular reflection $r_N \neq 0$ (dotted line), an Andreev reflection $r_A \neq 0$ (solid line), and a transmission

$t \neq 0$ (dashed line). This is consistent with the phase diagram of Fig. 4(a), which states that there is both transmission and Andreev reflection in this region (specular reflection is always possible). The state found in this case is plotted in Fig. 4(d), and the Andreev reflected wave is visible, as well as the transmitted bogolons.

The second case corresponds to an incident wave of positive energy $E = 1.8\Delta$, and an angle of incidence of $\theta_I = \pi/4$ (the set of green curves). The vertical gray line at this energy cuts only the normal reflection coefficient, whose norm is 1 because Andreev reflection and transmission coefficients are zero at this energy (for instance, the Andreev reflection coefficient decreases to 0 shortly after $E = \Delta/2$). For those experimental conditions, the phase diagram indeed tells us that there is no Andreev reflection nor transmission possible. The profile of this state is shown in Fig. 4(c). The wave at the Andreev frequency is evanescent in both regions, so the state is localized at the interface.

Finally, the third state corresponds to an incident energy $E = \Delta/2$ (within the gap) and an angle of incidence of $\theta_I = \pi/6$. The vertical gray line cuts only two blue lines: $r_N \neq 0$ and $r_A \neq 0$. There is no transmission ($|E| < \Delta$). The resulting state is shown in Fig. 4(b). We disregard the case of a wave coming from the superfluid toward the interface.

We note once again that a phase 2ϕ appears in the wave functions at the Andreev frequency (both in the reflected and transmitted wave) whereas there is no superfluid phase associated with the wave function at the pump frequency. This is known to occur in optical parametric amplification, as depicted in Fig. 5(b). The superfluid plays the role of a pump, the normal frequency is the source, and the Andreev frequency is the idler. From two pump particles, one gets one particle at each energy $E_p \pm E$, which verifies the energy and momentum conservation laws:

$$\begin{aligned} 2E_p &= (E_p + E) + (E_p - E), \\ 2i\phi &= 0 + ((-2\phi)i)^*, \end{aligned} \tag{45}$$

where the conjugation appears from Eq. (2).

IV. SIMULATIONS

To confirm that the reflection can be observed experimentally, we simulated the Gross-Pitaevskii equation (1) numerically. The parameters of the simulation are: $m = 8 \times 10^{-5} m_0$ (m_0 is the free electron mass), $\gamma = \hbar/2\tau$ with $\tau = 15$ ps, $\alpha = 3.6$ μeV · μm^2. We consider a 2D square area of 256 μm with a grid of 0.5 μm. The method used to integrate the Gross-Pitaevskii equation is the third-order Adams-Bashforth method [70]. The Laplacian is computed using the Fast Fourier Transform accelerated by the graphics processor unit [71].

A continuous wave (*cw*) pump under normal incidence covers a half-space $x > 0$. The pump energy E_p is 0.5 meV above the polariton energy at $k = 0$. We start with an initial condition $\psi(x, y, 0) = \psi_0 \mathcal{U}(x)$, where $\mathcal{U}$ is the Heaviside step function and ψ_0 is chosen so that $\alpha|\psi_0|^2 = 0.55$ meV [according to Eq. (6)], to reach the quasistationary regime faster. The density injected by the pump creates a gap in the bogolon spectrum $2\Delta \approx 0.5$ meV. Figure 6(a) shows the gapped

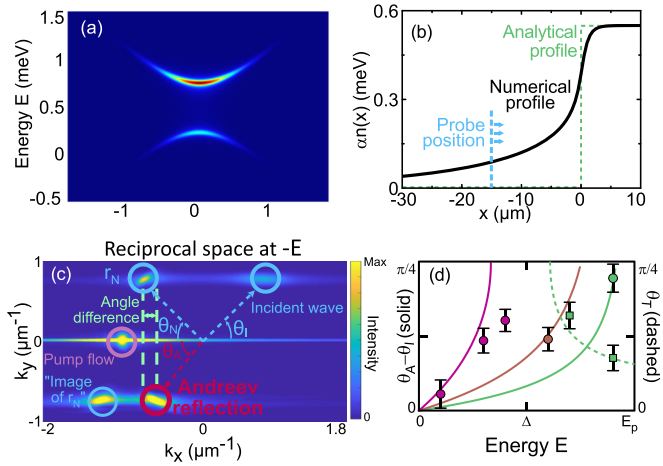

FIG. 6. (a) Bogolon dispersion in numerical experiments. Note the presence of a gap of 0.5 meV, as in the analytical calculations. (b) Numerical profile of the interactions $\alpha n(x)$ (black line). The plateau around 0.55 meV indicates the superfluid region. The analytical profile (step profile) is indicated as a green dashed line for comparison. The probe is located at 15 μm from the superfluid region (blue dashed line, the arrows indicate the direction of propagation of the probe, which is sent toward the superfluid). (c) The intensity distribution in the reciprocal space (measured in the N-region) at the "Andreev" frequency ($-E$ for an incident probe at $+E$) in a realistic configuration, where interactions are also present in the "normal" region. The angles are indicated directly in the figure, as done schematically in Fig. 2(c). The difference in k_x for normal and Andreev reflections is visible. (d) Left: Difference between the angle of incidence and the angle of Andreev reflection with respect to the energy for $\theta_I = \{45°, 20°, 10°\}$ (resp., purple/brown/green). Right axis: angle of transmission. Lines represent theory (solid for reflection angle, dashed for transmission angle) and points (circles/squares for reflection/transmission angles) results from numerical experiments. The error bars correspond to the reciprocal space broadening (full width half maximum).

bogolon spectrum in this pumped area, which is computed by sending a narrow pulse in space and time $\psi_0(x, y, t) = \exp[-(x^2 + y^2)/\sigma^2] \exp[-(t - t_0)^2/\tau^2]$, with $\sigma = 3$ μm, $\tau = 0.7$ ps, and $t_0 = 200$ ps (which allows the gapped superfluid density to settle down) into a system described by Eq. (1) with homogeneous pumping, triple-Fourier-transforming the result $\psi(x, y, t) \to \psi(k_x, k_y, E)$ over the final 150 ps containing the probe pulse (the whole simulation lasts 300 ps). Such gapped bogolon spectrum has been recently measured experimentally [55]. A crucial difference with respect to the ideal case we considered in the previous part, is that the superfluid flows out of the pumped region and its density in the normal region is nonzero, with a profile shown in Fig. 6(b). The superfluid injected at $k = 0$ by the pump creates a positive potential for itself (repulsive interactions). The repelled particles are accelerated and acquire a kinetic energy which progressively becomes equal to the pump energy E_p. The finite lifetime is responsible for the decay of the particles and sets the decay length of the density profile far from the interface in Fig. 6(b).

The main numerical experiment is based on having both the above-mentioned *cw* pump beam in the $x > 0$ region and

a *cw* probe beam sent from the normal region $x < 0$ at a given energy E (with respect to the pump energy E_p) and given angle of incidence (e.g., $\theta_I = 45^\circ$) toward the superfluid. The probe beam enters Eq. (1) similar to the pump beam, that is, as a term $+P_\mathrm{probe}\exp(-i\omega_\mathrm{probe}t)$, where $\omega_\mathrm{probe} = (E_p + E)/\hbar$ and $P_\mathrm{probe} = P_{0,\mathrm{probe}}\exp(-(x-x_0)^2/2\sigma^2_\mathrm{probe})\exp(-y/2\sigma^2_\mathrm{probe})$ with $P_{0,\mathrm{probe}} = 0.03P_0$ (the probe is much weaker than the pump), $\sigma_\mathrm{probe} = 10\,\mu\mathrm{m}$, $x_0 = 15\,\mu\mathrm{m}$. The probe needs to be sent from a reasonably short distance x_0 because of the polariton decay [the position is shown in Fig. 6(b)].

With respect to the ideal case previously considered, states in the normal region are not single particle states anymore but bogolon states with both positive and negative frequencies and opposite wave vectors. As shown below, this makes appear several features that are not present when the normal region is assumed empty. However, using energy and wave-vector resolution allows one to perfectly discriminate between different contributions.

Figure 6(c) shows, for the particular case of $E = 0.4\Delta = 0.1$ meV, the distribution of the probability density in the reciprocal space at the Andreev frequency (the conjugate of the frequency of the incident wave). This is obtained by making a triple Fourier transform of $\psi(x, y, t)\mathcal{U}(-x)f(t)$, where $\mathcal{U}$ is the Heaviside step function centered at the interface and $f(t)$ is a 500-ps-long time window. The whole simulation lasts 1000 ps; the first half is not used for the Fourier transform due to the transient behavior of the system.

We can see that the interactions in the normal region make appear several different intensity peaks not expected in the ideal picture considered analytically. First, the pump at the energy E_p is clearly visible at $-E$ because of its finite broadening due to the finite time window used in the simulation, but also due to nonlinear processes and finite lifetime effects. It is at $k_y = 0$, with a broadening along k_x. It shows a maximum at a negative k_x value, which corresponds to the superfluid particles accelerated by the abrupt density gradient at the interface. These particles ballistically propagate in the normal region with a maximal kinetic energy equal to E_p. Then, the incident wave is the only one in the positive k_x range. It is centered at the energy $+E$ but it remains visible in log scale at the energy $-E$. This allows us to well visualize the incident angle θ_I. At the same k_y as the incident wave, we see a trace of the normal reflection with the reflection angle θ_N. Again it is centered at $+E$ and is therefore only weakly visible at the energy $-E$. At k_y opposite to the normally reflected signal, we find two bright peaks which this time are centered at the energy $-E$. The one in red is the Andreev reflection. Its k_x is slightly different from the one of the normally reflected signal, as predicted analytically ($\theta_A \neq \theta_I$). Our simulations show that this small difference should be experimentally accessible: it becomes more important at larger energies and larger incidence angles [see Fig. 3(a)]. Finally, the last peak called "image of r_N" is the idler state of a parametric scattering process taking place in the normal region between the pump flow and the normally reflected signal (and thus r_N and "image of r_N" are symmetric with respect to the "Pump flow" label in the figure). This is a result of the deviation from the perfect interface picture, which (nicely enough) does not compromise the observation of the Andreev reflected signal as we further explain below. Complementary images, showing both frequencies $+E$ and $-E$ and both regions $x < 0$ and $x > 0$, and a comparison with a nonzero transmission case are provided in the Appendix.

As already stated, there is a flow at the pump energy in the normal region and a conversion from interaction to kinetic energy. This conversion defines a subsonic area, near the pump region, where the velocity of the superfluid is smaller than the one of bogolons $v < c$, and a supersonic region $v > c$. It can be shown (from $v = c \Longleftrightarrow mv^2/2 = \alpha n/2$ and energy conservation $mv^2/2 + \alpha n = E_p$) that the transition between both regions takes place when the interaction energy drops to two-thirds of the initial energy $\alpha n(x) = 2E_\mathrm{p}/3$. In the language of analog gravity [20] this frontier is an event horizon analog, with the supersonic region being the interior of the black hole. Similar schemes have been proposed in the past to study Hawking emission in polaritonic platform [21,72] and atomic condensates [22]. One can see in Fig. 6(b) that this boundary occurs very close to $x = 0$ (within 1 pixel of the numerical grid) and it is not expected, with the parameters chosen, to deeply modify the Andreev reflection scheme we studied in the previous section. Moreover, our probe corresponds to an excitation of the "superluminal" region of bogolon branch (as in Ref. [72]), for which propagation against the flow occurs even in the supersonic region, and where the propagation direction is not changing sign crossing the horizon. The elastic scattering toward the other bogolon branch propagating together with the flow occurs all along the propagation, because of the inhomogeneous density distribution. Independently of the strength of this scattering, because of the narrowness of this region, the probe (becoming a combination of propagative and evanescent waves) is still able to pass through the event horizon and to reach the gapped superfluid region, where it is entirely reflected by the gap, with both normal and Andreev components. The contribution of the evanescent waves of the gapped superfluid region into the reflection remains dominant, which justifies our simplified analytical treatment. Both the incident probe and the probe reflected at the gapped polariton fluid can provoke stimulated Hawking emission at the horizon. A vast majority of the signal reflected by the gapped fluid will pass through the horizon, but a tiny part will be reflected back to the gap as Hawking radiation, similar to multiple reflections occurring in other analog systems [73–76]. The detailed study of this last effect is beyond the scope of the present work and could be a topic for future studies.

We quantitatively verify the agreement between the analytical results of previous section and these numerical results in Fig. 6(d). Their reasonable agreement shows that the deviation from the ideal picture described above does not affect qualitatively the main features of the Andreev reflected signal. The difference between the angle of Andreev reflection and the angle of incidence is plotted with respect to the energy for different angles of incidence, showing both analytical results (lines) and numerics (points with error bars). We also plot the angle of transmission (dashed green line). We use the broadening (full width half maximum) of the peaks observed in the reciprocal space as an estimate for the uncertainty. Indeed, the shape of these peaks is asymmetric, and it is therefore not clear without a deep analysis, whether the "true" value of the wave vector corresponds to the maximum of the intensity, to the center of mass of the distribution, or to some other, more complicated quantity taking into account the different

nature of the sources of broadening (finite duration, finite system size, the shape of the dispersion relation...). Choosing the overall broadening for uncertainty guarantees that the real value of the wave vector falls inside the error bars. We can see that there is a good agreement between analytics and numerical experiments, even if the latter were performed in a realistic case (finite lifetime, pump flow in the normal region, etc.).

V. CONCLUSION

To conclude, we provide a comprehensive theoretical analysis of the angular-dependent Andreev reflection on a polaritonic gapped superfluid. For energies inside the gap, the superfluid hosts only evanescent states, whereas the non-superfluid region has propagative states. It enables us to observe a phenomenon analogous to the Andreev reflection: a wave incident at $+E$ is reflected at $-E$. The Andreev-reflected wave is reflected at an angle different from the angle of incidence. We find a critical angle, above which the Andreev reflection cancels and the Andreev wave becomes a surface mode. The Andreev reflection also occurs for energies outside the gap, accompanied by partial transmission into the superfluid. We find a good agreement between our analytical model and realistic numerical simulations. The phenomenon we describe is close to optical phase conjugation and analogous to reflection on black hole horizons (Hawking radiation). While most existing works only deal with Hawking radiation in 1D, our work could help working out its description in 2D. We believe that experimental observations could lead to new developments in the analog gravity community thanks to the strong similarities between Andreev reflection and Hawking radiation.

ACKNOWLEDGMENTS

We thank J. Meyer, A. Bramati, and D. Sanvitto for inspiring discussions. We thank all referees, whose remarkable involvement in the peer-review process allowed us to improve the quality and correctness of the manuscript. This research was supported by the ANR Labex GaNext (ANR-11-LABX-0014), the ANR program "Investissements d'Avenir" through the IDEX-ISITE initiative 16-IDEX-0001 (CAP 20-25), the ANR project "NEWAVE" (ANR-21-CE24-0019), and the European Union's Horizon 2020 program, through a FET Open research and innovation action under the Grant Agreement No. 964770 (TopoLight).

APPENDIX: ADDITIONAL NUMERICAL RESULTS

Here, we present additional results of numerical simulations for two particular cases of zero transmission at 45° incidence and nonzero transmission at 10° incidence, where it is allowed. To give a complete picture, for each of the two simulations we present the distribution of the probability density in the reciprocal space $|\psi(k_x, k_y)|^2$ both at the energy of the probe $+E$ and at the energy of the Andreev reflection $-E$. These distributions are presented both for the left and right half-spaces ($x < 0$ and $x > 0$). The values of the energies considered are $E = 0.05$ meV and $E = 0.4$ meV (with $E_p = 0.5$ meV and $\Delta = 0.25$ meV) for zero and nonzero transmission cases, respectively.

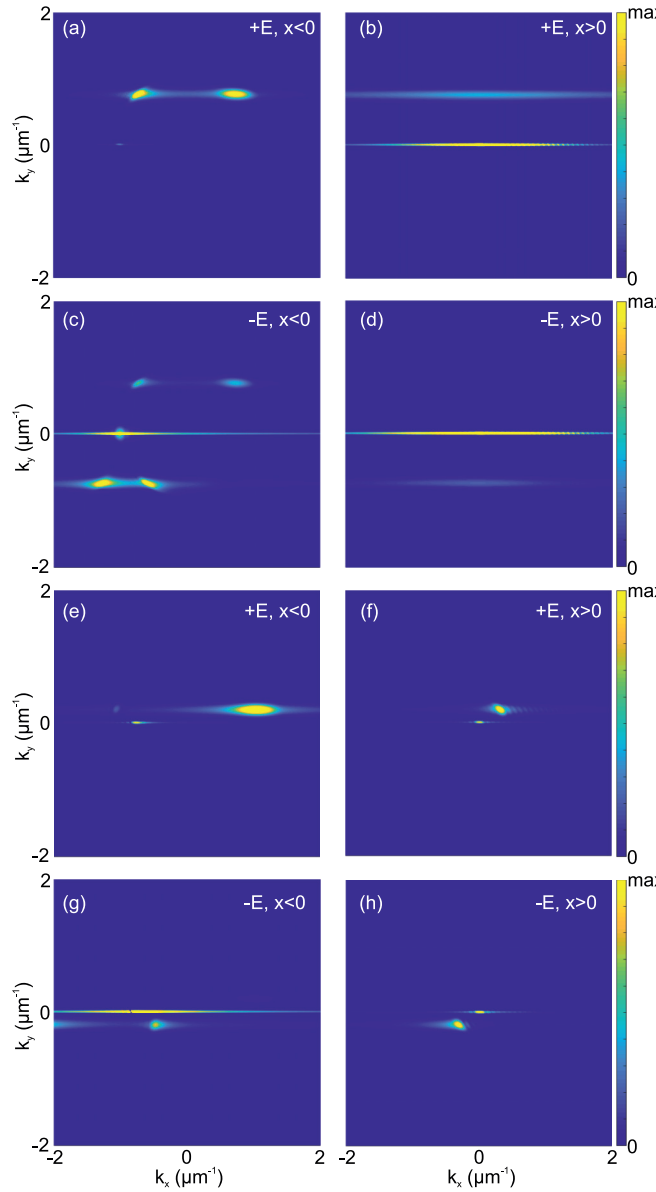

FIG. 7. Reciprocal space distribution for left (a, c, e, g: $x < 0$) and right (b, d, f, h: $x > 0$) half-spaces at the probe (a, b, e, f: $+E$) and conjugate (c, d, g, h: $-E$) energies, corresponding to zero (a,b,c,d: $E = 0.05$ meV) and nonzero (e, f, g, h: $E = 0.4$ meV) transmission. The color scale has been adjusted for visibility.

The results of these simulations are shown in Fig. 7. When the transmission is nonzero, a peak with a well-defined nonzero wave vector along k_x shows up in the reciprocal space [Figs. 7(f) and 7(h)]. On the contrary, when the transmission is zero, the spatially decaying bogolon solution shows up as a weak and broad maximum centered at $k_x = 0$ [Figs. 7(b) and 7(d)].

The region with the reflected signal $x < 0$ in Fig. 7 in both cases (zero and nonzero transmission) presents a nonzero signal both at the probe frequency and at the conjugate frequency, the latter corresponding to the Andreev reflection.

Since the probe intensity at the conjugate frequency $-E$ is especially weak, the maximum of the false color scale needs to be adjusted accordingly [Figs. 7(c) and 7(g)]. This makes the pump much more visible than at the probe frequency $+E$ [Figs. 7(a) and 7(e)]. The color scale is also adjusted between the top and the bottom panels.

[1] A. F. Andreev, Zh. Eksp. Teor. Fiz. **46**, 1823 (1964) [Sov. Phys. JETP **19**, 1228 (1964)].
[2] G. E. Blonder, M. Tinkham, and T. M. Klapwijk, Phys. Rev. B **25**, 4515 (1982).
[3] B. Pannetier and H. Courtois, J. Low Temp. Phys. **118**, 599 (2000).
[4] S. Bozhko, V. Tsoi, and S. Yakovlev, Pis'ma Zh. Eksp. Teor. Fiz. **36**, 123 (1982) [JETP Lett. **36**, 153 (1982)].
[5] P. A. M. Benistant, H. Van Kempen, and P. Wyder, Phys. Rev. Lett. **51**, 817 (1983).
[6] M. P. Enrico, S. N. Fisher, A. M. Guénault, G. R. Pickett, and K. Torizuka, Phys. Rev. Lett. **70**, 1846 (1993).
[7] B. V. Schaeybroeck and A. Lazarides, Phys. Rev. Lett. **98**, 170402 (2007).
[8] B. Van Schaeybroeck and A. Lazarides, Phys. Rev. A **79**, 053612 (2009).
[9] D. Husmann, S. Uchino, S. Krinner, M. Lebrat, T. Giamarchi, T. Esslinger, and J.-P. Brantut, Science **350**, 1498 (2015).
[10] C. W. J. Beenakker, Phys. Rev. Lett. **97**, 067007 (2006).
[11] A. Yariv, IEEE J. Quantum Electron. **14**, 650 (1978).
[12] H. Van Houten and C. Beenakker, Phys. B: Condens. Matter **175**, 187 (1991).
[13] J. C. J. Paasschens, M. J. M. de Jong, P. W. Brouwer, and C. W. J. Beenakker, Phys. Rev. A **56**, 4216 (1997).
[14] I. Zapata and F. Sols, Phys. Rev. Lett. **102**, 180405 (2009).
[15] I. Zapata, M. Albert, R. Parentani, and F. Sols, New J. Phys. **13**, 063048 (2011).
[16] T. Jacobson, Phys. Rev. D **53**, 7082 (1996).
[17] Z. Faraei and S. A. Jafari, Phys. Rev. B **100**, 245436 (2019).
[18] S. K. Manikandan and A. N. Jordan, Phys. Rev. D **96**, 124011 (2017).
[19] S. K. Manikandan and A. N. Jordan, Phys. Rev. D **102**, 064028 (2020).
[20] W. G. Unruh, Phys. Rev. Lett. **46**, 1351 (1981).
[21] D. D. Solnyshkov, H. Flayac, and G. Malpuech, Phys. Rev. B **84**, 233405 (2011).
[22] J. De Nova, D. Guéry-Odelin, F. Sols, and I. Zapata, New J. Phys. **16**, 123033 (2014).
[23] H. S. Nguyen, D. Gerace, I. Carusotto, D. Sanvitto, E. Galopin, A. Lemaître, I. Sagnes, J. Bloch, and A. Amo, Phys. Rev. Lett. **114**, 036402 (2015).
[24] J. R. Muñoz de Nova, K. Golubkov, V. I. Kolobov, and J. Steinhauer, Nature (London) **569**, 688 (2019).
[25] J. Drori, Y. Rosenberg, D. Bermudez, Y. Silberberg, and U. Leonhardt, Phys. Rev. Lett. **122**, 010404 (2019).
[26] V. I. Kolobov, K. Golubkov, J. R. Muñoz de Nova, and J. Steinhauer, Nat. Phys. **17**, 362 (2021).
[27] M. Jacquet, T. Boulier, F. Claude, A. Maître, E. Cancellieri, C. Adrados, A. Amo, S. Pigeon, Q. Glorieux, A. Bramati *et al.*, Phil. Trans. R. Soc. A. **378**, 20190225 (2020).
[28] M. J. Jacquet, L. Giacomelli, Q. Valnais, M. Joly, F. Claude, E. Giacobino, Q. Glorieux, I. Carusotto, and A. Bramati, Phys. Rev. Lett. **130**, 111501 (2023).
[29] A. Kavokin and G. Malpuech, *Cavity Polaritons* (Elsevier, Amsterdam, 2003).
[30] A. Baas, J. P. Karr, H. Eleuch, and E. Giacobino, Phys. Rev. A **69**, 023809 (2004).
[31] J. J. Hopfield, Phys. Rev. **112**, 1555 (1958).
[32] A. Kavokin, J. J. Baumberg, G. Malpuech, and F. P. Laussy, *Microcavities* (Oxford University Press, Oxford, UK, 2017).
[33] P. G. Savvidis, J. J. Baumberg, R. M. Stevenson, M. S. Skolnick, D. M. Whittaker, and J. S. Roberts, Phys. Rev. Lett. **84**, 1547 (2000).
[34] J. J. Baumberg, P. G. Savvidis, R. M. Stevenson, A. I. Tartakovskii, M. S. Skolnick, D. M. Whittaker, and J. S. Roberts, Phys. Rev. B **62**, R16247(R) (2000).
[35] P. G. Savvidis, C. Ciuti, J. J. Baumberg, D. M. Whittaker, M. S. Skolnick, and J. S. Roberts, Phys. Rev. B **64**, 075311 (2001).
[36] M. Saba, C. Ciuti, J. Bloch, V. Thierry-Mieg, R. André, L. S. Dang, S. Kundermann, A. Mura, G. Bongiovanni, J. L. Staehli *et al.*, Nature (London) **414**, 731 (2001).
[37] S. Kundermann, M. Saba, C. Ciuti, T. Guillet, U. Oesterle, J. L. Staehli, and B. Deveaud, Phys. Rev. Lett. **91**, 107402 (2003).
[38] A. A. Demenev, A. A. Shchekin, A. V. Larionov, S. S. Gavrilov, V. D. Kulakovskii, N. A. Gippius, and S. G. Tikhodeev, Phys. Rev. Lett. **101**, 136401 (2008).
[39] I. Septembre, S. Koniakhin, J. S. Meyer, D. D. Solnyshkov, and G. Malpuech, Phys. Rev. B **103**, 214504 (2021).
[40] D. D. Solnyshkov, G. Malpuech, P. St-Jean, S. Ravets, J. Bloch, and A. Amo, Opt. Mater. Express **11**, 1119 (2021).
[41] M. Richard, J. Kasprzak, R. André, R. Romestain, L. S. Dang, G. Malpuech, and A. Kavokin, Phys. Rev. B **72**, 201301(R) (2005).
[42] J. Kasprzak, M. Richard, S. Kundermann, A. Baas, P. Jeambrun, J. M. J. Keeling, F. M. Marchetti, M. H. Szymańska, R. André, J. L. Staehli *et al.*, Nature (London) **443**, 409 (2006).
[43] J. Keeling, F. Marchetti, M. Szymańska, and P. Littlewood, Semicond. Sci. Technol. **22**, R1 (2007).
[44] H. Deng, H. Haug, and Y. Yamamoto, Rev. Mod. Phys. **82**, 1489 (2010).
[45] T. Byrnes, N. Y. Kim, and Y. Yamamoto, Nat. Phys. **10**, 803 (2014).
[46] J. J. Baumberg, A. V. Kavokin, S. Christopoulos, A. J. D. Grundy, R. Butté, G. Christmann, D. D. Solnyshkov, G. Malpuech, G. Baldassarri Höger von Högersthal, E. Feltin *et al.*, Phys. Rev. Lett. **101**, 136409 (2008).
[47] F. Li, L. Orosz, O. Kamoun, S. Bouchoule, C. Brimont, P. Disseix, T. Guillet, X. Lafosse, M. Leroux, J. Leymarie *et al.*, Phys. Rev. Lett. **110**, 196406 (2013).
[48] J. D. Plumhof, T. Stöferle, L. Mai, U. Scherf, and R. F. Mahrt, Nat. Mater. **13**, 247 (2014).
[49] M. Dusel, S. Betzold, O. A. Egorov, S. Klembt, J. Ohmer, U. Fischer, S. Höfling, and C. Schneider, Nat. Commun. **11**, 2863 (2020).
[50] J. Tang, J. Zhang, Y. Lv, H. Wang, F. F. Xu, C. Zhang, L. Sun, J. Yao, and Y. S. Zhao, Nat. Commun. **12**, 3265 (2021).

[51] I. Carusotto and C. Ciuti, Phys. Rev. Lett. **93**, 166401 (2004).
[52] C. Ciuti and I. Carusotto, Phys. Status Solidi B **242**, 2224 (2005).
[53] I. Carusotto and C. Ciuti, Rev. Mod. Phys. **85**, 299 (2013).
[54] R. Juggins, J. Keeling, and M. Szymańska, Nat. Commun. **9**, 4062 (2018).
[55] F. Claude, M. J. Jacquet, I. Carusotto, Q. Glorieux, E. Giacobino, and A. Bramati, Phys. Rev. B **107**, 174507 (2023).
[56] E. Cancellieri, F. M. Marchetti, M. H. Szymańska, and C. Tejedor, Phys. Rev. B **82**, 224512 (2010).
[57] A. Berceanu, E. Cancellieri, and F. Marchetti, J. Phys.: Condens. Matter **24**, 235802 (2012).
[58] I. Septembre, J. S. Meyer, D. D. Solnyshkov, and G. Malpuech, Phys. Rev. B **107**, 165301 (2023).
[59] V. Goblot, H. S. Nguyen, I. Carusotto, E. Galopin, A. Lemaître, I. Sagnes, A. Amo, and J. Bloch, Phys. Rev. Lett. **117**, 217401 (2016).
[60] W. Voigt, Philos. Mag. Ser. **4**, 90 (1902).
[61] B. Zhen, C. W. Hsu, Y. Igarashi, L. Lu, I. Kaminer, A. Pick, S.-L. Chua, J. D. Joannopoulos, and M. Soljačić, Nature (London) **525**, 354 (2015).
[62] A. Cerjan, S. Huang, M. Wang, K. P. Chen, Y. Chong, and M. C. Rechtsman, Nat. Photon. **13**, 623 (2019).
[63] S. Richter, H.-G. Zirnstein, J. Zúñiga Pérez, E. Krüger, C. Deparis, L. Trefflich, C. Sturm, B. Rosenow, M. Grundmann, and R. Schmidt-Grund, Phys. Rev. Lett. **123**, 227401 (2019).
[64] R. L. Mc Guinness and P. R. Eastham, Phys. Rev. Res. **2**, 043268 (2020).
[65] Z.-w. Li, J.-j. Liu, Z.-G. Chen, W. Tang, A. Chen, B. Liang, G. Ma, and J.-c. Cheng, Phys. Rev. Lett. **129**, 084301 (2022).
[66] M. Król, I. Septembre, P. Oliwa, M. Kędziora, K. Łempicka-Mirek, M. Muszyński, R. Mazur, P. Morawiak, W. Piecek, P. Kula *et al.*, Nat. Commun. **13**, 5340 (2022).
[67] V. V. Cheianov, V. Fal'ko, and B. Altshuler, Science **315**, 1252 (2007).
[68] Y. Betancur-Ocampo, F. Leyvraz, and T. Stegmann, Nano Lett. **19**, 7760 (2019).
[69] F. Goos and H. Hänchen, Ann. Phys. **436**, 333 (1947).
[70] F. Bashforth and J. C. Adams, *An Attempt to test the Theories of Capillary Action by comparing the theoretical and measured forms of drops of fluid* (Kessinger Publishing, LLC, Whitefish, MT, 1883).
[71] J. Reese and S. Zaranek, GPU Programming in MATLAB, https://www.mathworks.com/company/newsletters/articles/gpu-programming-in-matlab.html, accessed: 30/05/2023.
[72] D. Gerace and I. Carusotto, Phys. Rev. B **86**, 144505 (2012).
[73] S. Corley and T. Jacobson, Phys. Rev. D **59**, 124011 (1999).
[74] A. Coutant and R. Parentani, Phys. Rev. D **81**, 084042 (2010).
[75] J. Steinhauer, Nat. Phys. **10**, 864 (2014).
[76] C. Peloquin, L.-P. Euvé, T. Philbin, and G. Rousseaux, Phys. Rev. D **93**, 084032 (2016).